J Appl Electrochem (2010) 40:123–131
DOI 10.1007/s10800-009-9988-x

ORIGINAL PAPER

Transient film formation on chalcopyrite in acidic solutions

C. A. C. Sequeira · D. M. F. Santos

Received: 23 March 2009 / Accepted: 16 August 2009 / Published online: 2 September 2009

Abstract The transient time-dependent region characteristic of the anodic passive film formation on chalcopyrite in sulphuric acid solutions was studied by galvanostatic measurements. The occurrence of two passivation subregions was observed. Both followed the Sato–Cohen (logarithmic) model for the growth of anodic passive films. The experimental electric field for the two passivated steps was approximately 10^5 V cm^{-1}. The electric field for the first step, at lower potentials, decreased with increasing ionic strength, but was pH independent. In the second step, the electric field decreased with increasing pH. The Tafel relationship was followed for constant electrical charge passed. The transition points between first and second step had almost the same electrical charge for different current densities and the electrical charge of the transition point decreased with increasing pH. The effects of temperature and iron/copper ion additions were also studied.

Keywords Chalcopyrite · Sulphuric acid · Galvanostatic technique · Anodic passivation · Kinetic model

1 Introduction

The major source of copper, chalcopyrite, is mainly converted to the metal by pyrometallurgical processes that also produce gaseous sulphur dioxide [1, 2]. The environmental requirements being imposed on sulphide smelters have led to a greater effort to develop hydrometallurgical routes for the treatment of sulphides, in order to avoid the evolution of sulphur dioxide [3–8]. These processes involve the oxidation of sulphides to elemental sulphur or sulphate either using oxidants such as oxygen, ferric ion, and cupric ion [9–16] or by direct electrolysis [13, 14, 17–19]. The oxidation of sulphides can be regarded as an electrochemical reaction with the cathodic reduction of the oxidant and the anodic oxidation of the sulphides [20–22].

Essentially, natural chalcopyrite is an n-type semiconductor [23–27] whose band gap is 0.60 eV with a resistivity of approximately 2×10^{-4} to 9×10^{-3} Ω m and could be variable in stoichiometry and/or impurities. Ionically, chalcopyrite should be considered as $Cu^{+}Fe^{3+}(S^{2-})_2$ rather than $Cu^{2+}Fe^{2+}(S^{2-})_2$ [27]. Chalcopyrite does not have a wide stability range in the Cu–Fe–S system, and associated equilibrium phases, with their normal compositions, include cubanite ($CuFe_2S_3$), talnakhite ($Cu_9Fe_8S_{16}$), mooihoekite ($Cu_9Fe_9S_{16}$), haycockite ($Cu_4Fe_5S_8$) and perhaps bornite (Cu_5FeS_4) [28]. The principal donor defect in natural chalcopyrite is a metal interstitial, making it metal excess in composition. Several reports on the anodic behaviour of chalcopyrite are available [17, 19, 29–36].

Earlier studies conducted on the anodic dissolution of chalcopyrite [6] found two regions in the anodic polarisation curves; at low potentials (0.8 V vs. SHE) the current is time dependent, whereas, it is time independent at higher potentials. In the first region covellite, CuS, appeared, corresponding to the preferential dissolution of iron. The oxidation of covellite was slow at low temperatures. Also, they show that the time dependence of the current in the low-current region is indicative of a rate controlling diffusion process such as metal ions out of the surface. However, in the high-current region where the current is time independent, it is possible that the formation of holes

C. A. C. Sequeira (✉) · D. M. F. Santos
Materials Electrochemistry Group, Instituto Superior Técnico, TU Lisbon, Av. Rovisco Pais, 1049-001 Lisbon, Portugal
e-mail: cesarsequeira@ist.utl.pt

is rate determining. The potential exerted by a ferric sulphate solution (0.75 V vs. SHE) lies just within the low-current region resulting in a time-dependent process [30]. Warren et al. also found two regions in the acid system [19]. The initial formation of a defect intermediate, deficient in iron, was proposed to occur at low potentials. At higher potentials, the corrosion current is much greater and results in the formation of elemental sulphur and sulphate.

Biegler and Swift found a first step which represents a surface oxidation process involving a thin surface layer of metal-deficient chalcopyrite [17]. The potential range of 0.4–0.8 V (vs. SHE) associated with this step covers the potential range expected in the ferric ion leaching of copper sulphide ores; therefore, identification of this reaction has important practical implications. The second step, for potentials $\geq$1 V vs. SHE, is also an anodic reaction in which equimolar quantities of the two metal ions (Cu^{2+} and Fe^{3+}) are produced. Approximately 14% of the sulphur in chalcopyrite is oxidised to sulphate and 86% to elemental sulphur. They also found a critical potential of $\sim$1.0 V vs. SHE in 1 M H_2SO_4 solution. Below this critical potential, the current was observed to decay with time, and above that potential the current is almost constant. This behaviour was related to the number of corrosion sites, which increased dramatically as the potential was increased [17].

Current focus is already too long and, although there is a need to pursue the research on the reaction kinetics and mechanisms of chalcopyrite leaching [7, 37], the present study is intended to identify the transient time-dependent region of chalcopyrite in sulphuric acid solutions and to establish the kinetics of anodic film formation in the transient state. In this way, it is hoped to contribute to the knowledge of chalcopyrite hydrometallurgy, using an electrochemical focus to elucidate the passive anodic behaviour of this mineral.

2 Experimental

The electrochemical cell was a typical three electrode system (chalcopyrite working electrode, graphite counter electrode and saturated calomel or silver chloride reference electrode). The counter electrode was separated from the bulk electrolyte by a porous glass frit. Potential measurements between working and reference electrode were made through a Luggin capillary that was placed as close as possible to the surface of the working electrode. All potentials reported are referred to the standard hydrogen electrode (SHE).

A Princeton potentiostat model 173, potential sweep generator model 175, Houston X-Y plotter 2000 and a ten channel recorder were employed for the experiments. The study was performed using a galvanostatic technique.

Table 1 Analysis of Pima concentrate

Chemical analysis		Mineralogical analysis	
Element	%	Mineral	%
Cu	27.2	$CuFeS_2$	80
Fe	29.2	FeS_2	5
S	30.8	SiO_2	5
Sb	0.60	Al_2O_3	0.93
Zn	0.50	CaO	0.52
Mo	0.14	Talc and chlorite	8
Pb	0.07		
As	0.02		

The working electrodes were prepared from chalcopyrite obtained from Pima flotation concentrate. The chemical and mineralogical analysis of chalcopyrite concentrate as received, using ICP and XRD and verified by the Rietveld method [38], is shown in Table 1.

Chalcopyrite was cut with a diamond saw and mounted in epoxy resin. The shape of the sample was generally rectangular, with an exposed area close to 1 cm^2, which remained essentially constant after repeated polishing. A small hole was drilled into the back of the mounted samples and silicone glue was used to seal a glass tube inserted into the hole. Electrical contact was made by dropping a small amount of mercury into the glass tube and inserting a platinum wire. Before each experiment, samples were hand polished through four grit sizes of silicon carbide paper with a final polish using an abrasive 6 μm diamond spray. Copper and iron in solution were measured by atomic absorption spectrophotometry and elemental sulphur was measured by CS_2 extraction and evaporation. Deionised water and reagent grade chemicals were used to prepare all aqueous solutions.

3 Results

The chalcopyrite sample contains 5% pyrite, which is not as passive as often claimed, especially above $\sim$0.6 V vs. SCE, which could influence the present data, in light of recent publications by Dixon et al. on the Galvanox process [39]. Therefore, preliminary galvanostatic oxidation curves were obtained with nearly pure chalcopyrite, being concluded that the 5% pyrite content of the tested electrodes has no effect on the rate of chalcopyrite oxidation, at least for the present range of potentials. Typical galvanostatic oxidation curves (potential vs. time) for our chalcopyrite sample, are shown in Fig. 1. The region in which the potential increases with time is defined as the transient time-dependent region and the plateau region as the steady

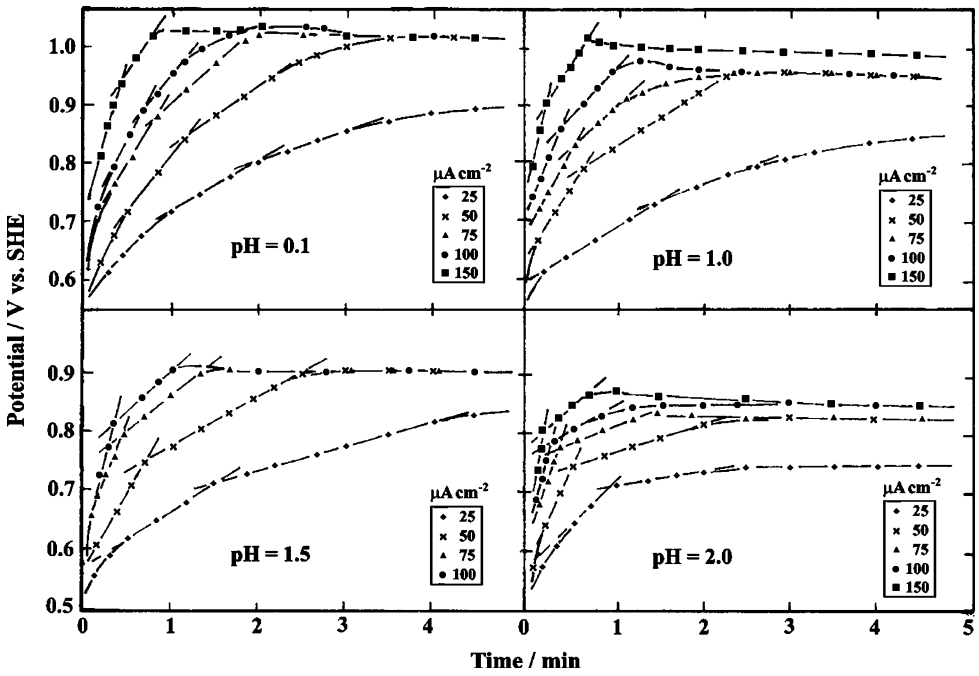

Fig. 1 Galvanostatic oxidation curves for chalcopyrite at various pH and current densities, 25 °C

state time-independent region. It is useful to consider these two regions separately.

The transient time-dependent region is related with the anodic film formation in which the extent of film dissolution with time is negligible (generally data between 0.7 and 0.9 V vs. SHE). In order to study the transient time-dependent region, the effects of current density, pH, applied current, copper/iron ions addition and temperature were considered.

3.1 Effect of current density

As shown in Fig. 1, after an initial short and nonlinear rise, the potential increases linearly with time for all current densities. The linear region shows two steps and the slope of the first step is greater than the second. The same behaviour was observed for different acidities as also illustrated in Fig. 1. In general, the slope of the first step is greater for lower acidities at constant current density, while the second step shows the opposite. Figure 2 shows this tendency at 50 μA cm^{-2}. It is worth noting that the ionic strength was not constant for different acidities.

3.2 Effect of pH at constant ionic strength

Figure 3 shows galvanostatic oxidation curves at constant ionic strength for different acidities. Magnesium sulphate was used to keep the ionic strength at a value of 3.0. At lower potential (first step), the oxidation of chalcopyrite seems to be independent of the pH. On the other hand, Fig. 2 shows that the ionic strength has little effect in this

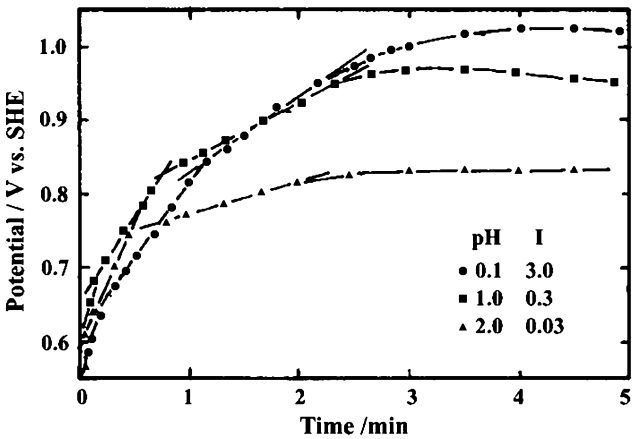

Fig. 2 Galvanostatic oxidation curves at 50 μA cm^{-2} for different pH and ionic strength, 25 °C

region. At higher potential, second step galvanostatic curves are acid dependent, increasing the potential with acidity. Chemical analysis for iron and copper in the solution used for the first step galvanostatic curves also confirmed that an increase in the solution pH from about 0.1–2.8 results in an insignificant increase in the chalcopyrite conversion rate.

3.3 Effect of the applied current

Figure 4 shows a galvanostatic oxidation curve for chalcopyrite in which the applied current density (10 μA cm^{-2}) at steady state, was suddenly changed to 100 μA cm^{-2}. After it

reached the steady state, the original current density (10 μA cm^{-2}) was applied again. The final potential in the three regions was approximately the same.

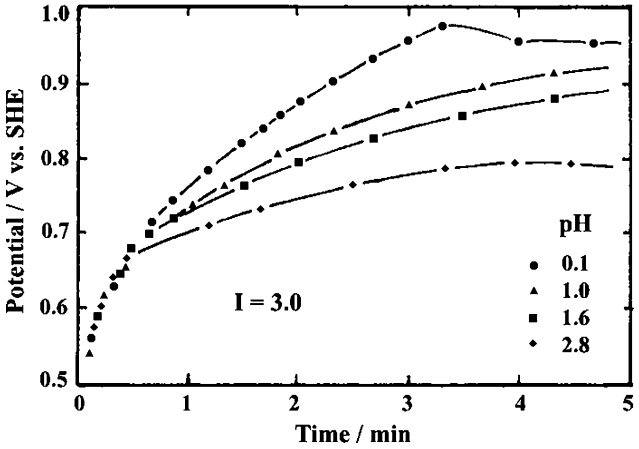

Fig. 3 Effect of pH on anodic film growth at constant ionic strength, 50 μA cm^{-2}, 25 °C

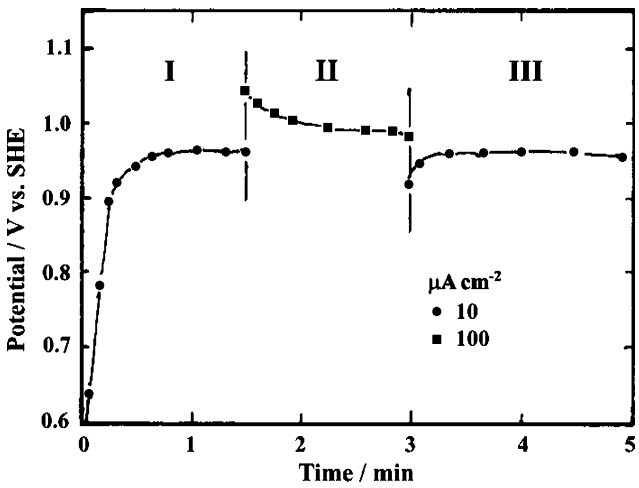

Fig. 4 Effect of the external applied current, pH 0.1 (1.0 M H_2SO_4), 25 °C

3.4 Effect of copper/iron ions addition

Since cupric and ferrous ions might be expected as products of the oxidation of chalcopyrite, the effect of addition of these ions on the galvanostatic polarisation curves was investigated and the results are shown in Fig. 5.

Addition of copper up to 10 g dm^{-3} has little or no effect. Figure 5 shows that for a given applied current density, the steady state potential, independent of time, is reached more rapidly at lower concentrations of ferrous ions. Addition of ferrous ion up to 1.0 g dm^{-3} has no effect, but for higher concentrations galvanostatic curves show a plateau value at approximately 0.7 V vs. SHE.

3.5 Effect of temperature

The effect of temperature on the anodic behaviour of chalcopyrite was studied in 1 M H_2SO_4 with current density of 25 μA cm^{-2}. The shape of all galvanostatic curves in the transient time-dependent region is the same. Figure 6 shows that the potential decreases with increasing temperature. Experiments up to 45 °C show little temperature effect in anodic film formation at constant current. It should be noted that all samples exhibited passive like response during the entire galvanostatic experiments. Consequently, atomic absorption spectrophotometry assays showed that the concentration of copper and iron due to the dissolution of the electrode submitted to the entire polarisation were, in average, as low as ~4 μM at 15 °C and 40 μM at 50 °C.

4 Discussion

The growth of anodic passive films on metals may follow different rate laws at different temperatures. The parabolic law, characteristic of thick films formed at high temperatures, is adequately explained by the Wagner theory [40, 41] which assumes that the rate controlling step of the process is the diffusion of ions through the film to the

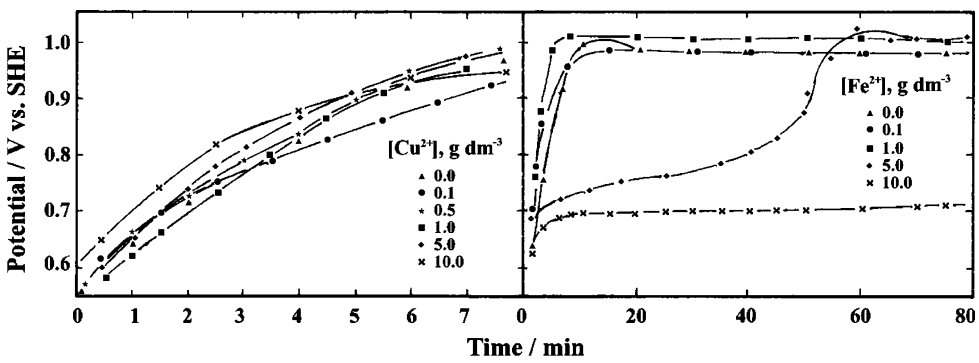

Fig. 5 Plot of potential versus time at various cupric and ferrous ion additions, pH 0.1 (1.0 M H_2SO_4), 25 μA cm^{-2}, 25 °C

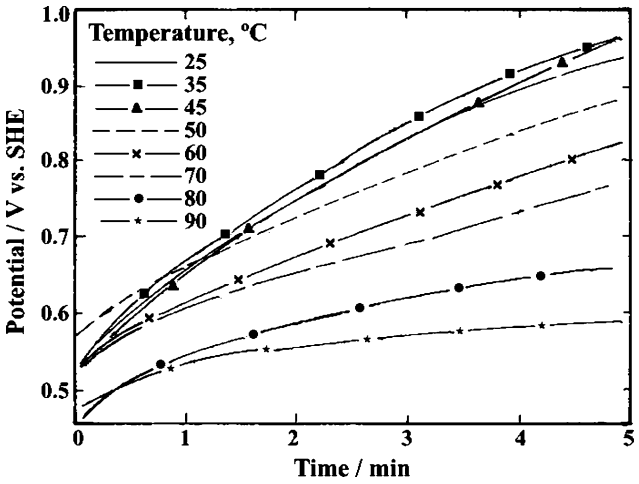

Fig. 6 Effect of temperature, pH 0.1 (1.0 M H_2SO_4), 25 μA cm^{-2}

reaction interface. The logarithmic rate law observed for the formation of thin films at low temperatures, on the other hand, is not so fully understood [35, 42–44].

Cabrera and Mott explained the logarithmic law for oxide film formation, whose basic postulate is that the rate determining step is the transfer of ions across an interface [45]. A strong electric field produced by a layer of adsorbed oxygen ions at the film/atmosphere interface lowers the energy barrier for ionic diffusion. Under the influence of this field, of the order of 10^6 V cm^{-1}, the motion of ions is shown to be overwhelming in the direction of the field, with the number of jumps in the reverse direction being negligible. The rate of film growth is determined by the rate at which ions jump from the adsorbed oxygen layer into the film under the influence of the electric field [46–48].

The rate equation derived by Cabrera and Mott [45] for this process is:

$$\frac{dx}{dt} = vNv \exp - \left(\frac{W - q\lambda E}{kT}\right) \quad (1)$$

where v is the vibration frequency, x is the film thickness, N is the number of atoms per cm^2 in position to jump into the film, v is the volume of thin film per metal ion, W is the activation energy, q is the charge of the ion, λ is the distance from the lattice position of a metal to the first interstitial lattice position in the thin film and E is the electrical field.

An approximate integration of Eq. 1, valid only for $q\lambda E/kT \gg 1$, gives the reciprocal logarithmic tarnishing law [49]:

$$\frac{1}{x} = A' - B' \ln t \quad (2)$$

where A' and B' are constants for a given average value of the thickness of the layer and temperature.

One consequence of the logarithmic law is that the growth rate is initially very fast, but decreases rapidly so that the film approaches a limiting thickness, in which the increase in its thickness with time is so slight that it is practically unobservable. In this connection, Cabrera and Mott [45] compared their theoretical treatment with the experimental results. They found an exponential dependence of the current on the field strength, E:

$$i = \alpha_0 \exp(\beta_0 E) \quad (3)$$

where i is the external current, and α_0 and β_0 are parameters related to the initial oxidation stage. Sato and Cohen [50] measured the rate of anodic passive film growth on iron in a neutral borate-boric acid buffer solution as a function of the electrode potential and film thickness. The observed kinetics followed the empirical equation

$$i = \alpha \exp(\beta V - \beta' Q) \quad (4)$$

where V is the potential between the working and the reference electrodes, Q is the accumulated charge in the thin film, and α, β and β' are parameters.

Equation 4 was then derived theoretically on the basis of a place exchange mechanism. According to the mechanism, a layer of oxygen (or another gaseous oxidant) is adsorbed onto the surface which then exchanges places with underlying metal atoms. A second layer of gas is then adsorbed and the two metal-oxidant pairs rotate simultaneously. This process is repeated and results in film thickening. This place exchange mechanism was used to derive equations which conform to experimental results on iron. The general treatment is based on theory of anodic film formation for high-electric field ionic conductivity [41, 51]. Ionic conductivity in crystalline solids occurs through the movement of defects in the lattice. One of these defects is the interstitial metal ions moving through the interstices of a network of immobile metal and oxygen atoms. The exponential term of Eq. 1 represents the fraction of ions which have sufficient energy to surmount the potential energy barrier, W. The electric field is assumed to reduce the height of the energy barrier from W to $W - q\lambda E$ for ions moving with the electric field, E, and to increase the barrier for ions moving against the electric field. If the fraction of ions is very small, due to a large activation energy or low temperature, the rate may be so small that the process could be considered as not occurring at all.

The anodic dissolution of a metal sulphide can be briefly expressed according to Eq. 5,

$$MS \leftrightarrows M^{2+} + S^0 + 2e^- \quad (5)$$

and charge transfer at the metal sulphide/solution interface may be expressed quantitatively by the Butler–Volmer equation (Eq. 6), which describes the current–potential

dependence for the case of pure charge transfer overpotential for a single electron transfer process

$$i = nFk_a \exp\left(\frac{\beta FV}{RT}\right) - nFk_c(M^{2+}) \exp\left[\frac{-(1-\beta^0)FV}{RT}\right] \quad (6)$$

where the first term of the equation is the anodic partial current density and the second term is the cathodic partial current density, being F the Faraday constant, β^0 the transfer coefficient and k_a and k_c the rate constants for the anodic and cathodic directions, respectively, in the absence of a potential bias. Concepts developed in the field of corrosion may be applied to the leaching of electron conducting solids in hydrometallurgical systems. For this reason, the anodic dissolution rate of chalcopyrite may be called the corrosion current [4, 52, 53].

During anodic film formation at constant current, each new layer requires an extra potential to be added across the film to maintain constant electric field in the layer and, hence, the current. The relation between the rate of potential increase and the current density is derived as follows. The rate of thickness increase is given by

$$\frac{dx}{dt} = \frac{iM}{nF\rho} \quad (7)$$

where t is the time, i is the ionic current density to form the anodic film, n is the number of Faraday (F) required to form the molecular weight of a compound M and ρ is the film density.

Equation 7 assumes that the applied constant current is entirely used to grow the anodic film. If dV/dx, which is the electric field, does not vary with increasing thickness of a compound at constant ionic current density, the rate of potential increase is described by Eq. 8.

$$\frac{dV}{dt} = \frac{dV}{dx}\frac{dx}{dt} = \frac{EiM}{nF\rho} \quad (8)$$

Table 2 shows the values of the two slopes $\Delta V/\Delta t$, for each current density and pH obtained from Fig. 1.

Table 2 Values of two slopes $\Delta V/\Delta t$ from galvanostatic oxidation curves at different pH

Current density ($\mu A\ cm^{-2}$)	Slopes: $\Delta V/\Delta t$ ($mV\ s^{-1}$)							
	pH 0.1		pH 1.0		pH 1.5		pH 2.0	
	1st	2nd	1st	2nd	1st	2nd	1st	2nd
25	1.42	0.92	1.83	1.17	1.6	0.75	2.17	0.38
50	3.17	1.80	4.00	1.59	5.0	1.43	5.50	0.80
75	4.00	2.40	5.00	2.33	6.5	1.83	7.00	0.95
100	5.33	3.50	5.66	3.13	9.0	2.38	9.50	1.33
150	8.00	5.33	9.50	4.40			13.9	2.26

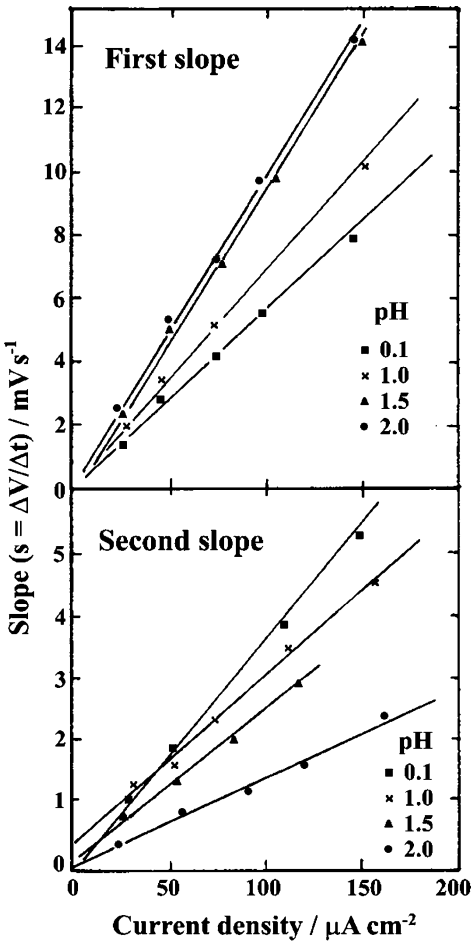

Fig. 7 Dependence of the slopes $\Delta V/\Delta t$ on current density at various acidities, 25 °C (Sato–Cohen model)

The dependence of slopes in V versus t on current density at different acidities is shown in Fig. 7.

The linear relationship between potential/time versus current density can be expressed by Eq. 9

$$\frac{\Delta V}{\Delta t} = S = a + b'i \quad (9)$$

where b' varies with the pH. The intercept, a, is close to zero. The combination of Eqs. 8 and 9 gives

$$b' = f(\text{pH}) = \frac{EM}{nF\rho} \quad (10)$$

Table 3 shows the values of b' for the two slopes at different pH.

The Cabrera–Mott model (Eq. 3) may be rewritten, giving

$$V = \frac{it}{\gamma}\log\left(\frac{i}{\alpha_0}\right) + V_0 \quad (11)$$

where γ relates thickness with electric charge passed and V_0 is the rest potential of chalcopyrite. Equation 11 is a

Table 3 Values of b' for the two slopes in V/t on current density at different acidities

pH	1st slope		2nd slope	
	b' (mV cm^2 A^{-1} s^{-1})	a (mV s^{-1})	b' (mV cm^2 A^{-1} s^{-1})	a (mV s^{-1})
0.1	0.051	0.29	0.035	−0.34
1.0	0.058	0.59	0.027	0.39
1.5	0.095	−0.40	0.021	0.28
2.0	0.092	0.28	0.015	−0.03

linear function between V and t at constant current, with a slope of:

$$S = \frac{i}{\gamma}\log\left(\frac{i}{\alpha_0}\right) \tag{12}$$

In Fig. 8, experimental values of S/i versus log i do not fit with the Cabrera–Mott model. Equation 4 that represents the Sato–Cohen model, may be rewritten as

$$V = \frac{\beta'}{\beta}it + \frac{1}{\beta}\log\frac{i}{\alpha} \tag{13}$$

At constant current density, the potential is a linear function of time with a slope of

$$S = \frac{\beta'}{\beta}i = b\prime i \tag{14}$$

Such a plot was made in Fig. 7. The results follow the Sato–Cohen model.

The galvanostatic curves at constant electrical charge, Q, should be straight lines according to the Sato–Cohen model. The slope should be the same for different values of total charge passed. Potentials estimated at different film thickness (charge density in μC cm^{-2}) in the V–t curves in Fig. 1 are plotted as a function of the logarithm of the current density in Fig. 9 for different acidities. The polarisation curves thus obtained for the linear region of the transient state give straight lines of almost constant slope, obeying the Tafel relationship (Eq. 15).

$$i = \alpha\,\exp(\beta V) \tag{15}$$

where α and β are constants. β is independent of the film thickness and its estimated value is 19 V^{-1} at pH 0.08, which is very close to that obtained by Sato–Cohen (19.2 V^{-1}) [50] and Chao–Lin–MacDonald (20 V^{-1}) [54] models. At higher pH, β varies between 12 and 19 V^{-1} which indicates that there is no appreciable effect of pH on the charge transfer process. The intercept α decreased with increasing film thickness. The pH dependence of the parameters can be rationalised due to transfer of solution OH^- ions to O in the metal-deficient sulphide layer.

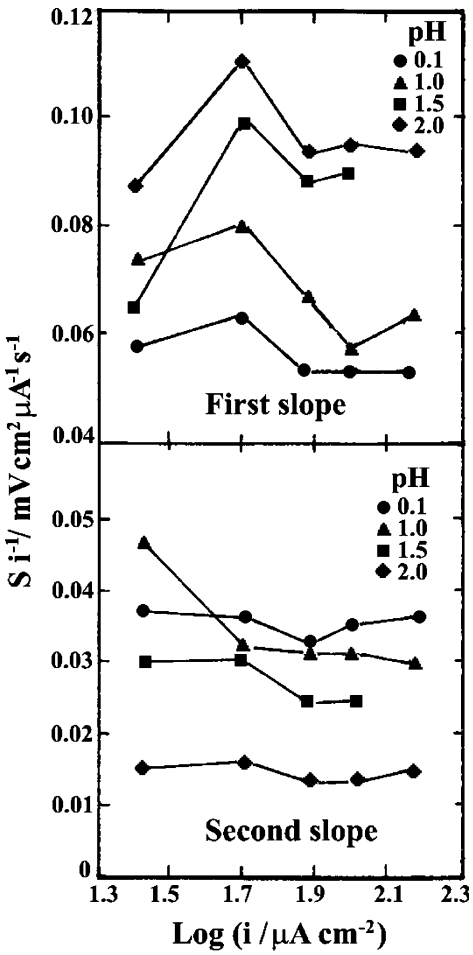

Fig. 8 Relationships of the $\Delta V/\Delta t$ slopes over i on log i at different acidities, 25 °C (Cabrera–Mott model)

The Cabrera–Mott model (Eq. 3) may be rewritten in the form of Eq. 16.

$$\log i = \frac{\gamma\Delta V}{Q} + \log\,\alpha_0 \tag{16}$$

A plot of log i versus ΔV should have a slope of γ/Q. For different thicknesses the slope is variable and therefore, this model does not fit the experimental values.

Table 4 shows the total electrical charge values, Q, for points of intersection of the two slopes obtained from Fig. 1. The total electrical charge at these points of intersection is approximately the same for different current densities at constant pH, so that potential-curve values on those points must follow the Tafel relationship (Eq. 15), which was obtained for the transient state region at constant total electrical charge. Figure 10 shows the logarithm of the current density as a function of potential for these particular points.

The polarisation curves at different acidities all follow the Tafel equation. It is worth noting that the transition between the first and second slope requires a constant film

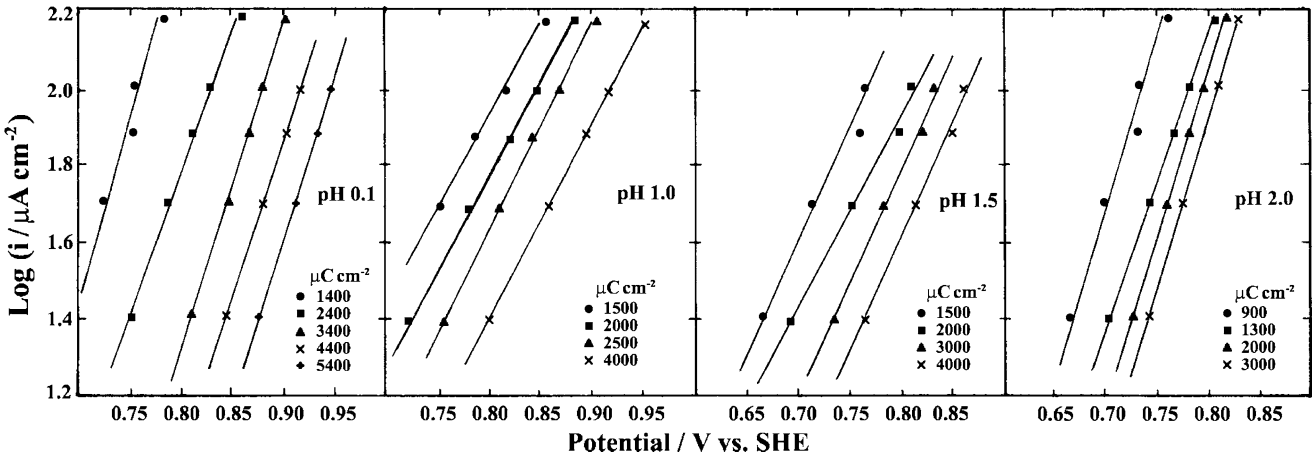

Fig. 9 Polarisation curves at various electric charge and pH values, 25 °C

Table 4 Total electrical charge, Q (in μC cm^{-2}), for points of intersection of the two slopes $\Delta V/\Delta t$

Current density (μA cm^{-2})	pH			
	0.1	1.0	1.5	2.0
25	3375	2000	2250	1500
50	3500	2000	2000	1500
75	3600	2400	1875	1300
100	3500	2000	2000	1500
150	3600	2250		1500

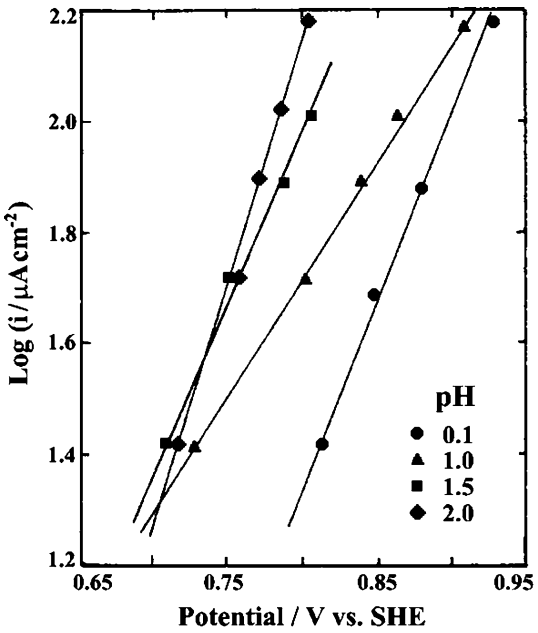

Fig. 10 Polarisation curves for points of intersection of the two slopes $\Delta V/\Delta t$ at various acidities, 25 °C

thickness, for the same pH. The film thickness is thinner at lower acidities.

This transient state is equivalent to the passive region observed in potentiodynamic experiments [19] in which the presence of the passive region is attributed to the formation of a thin layer on the surface.

5 Conclusions

Galvanostatic curves (potential vs. time) show two regions: the transient state which is related to anodic positive film formation; and the steady state, which is represented by a levelling off of the potential. The latter corresponds to the condition where the corrosion current is equal to the applied current, resulting in a film thickness of constant value. This research was focused on the study of the anodic film formation on chalcopyrite in the transient state.

The transient state shows two steps. Both follow the Sato–Cohen model for the growth of anodic passive films. The first, at lower potentials, shows a slope greater than the second, which occurs at higher potentials. The Sato–Cohen (logarithmic) model for solid film formation was also proposed by Warren et al. [19] based on current decay measurements at constant potential in the potential-passive region of chalcopyrite in acid solutions.

The experimental electric field value for the first passivation region is approximately 10^5 V cm^{-1}, increasing with the decreased ionic strength. The electric field created by the second passivation region is approximately 10^5 V cm^{-1} and decreases with increasing pH. In general, the transient state region follows the Tafel relationship for constant total electrical charge passed, Q. The transition points between the first and second step have almost the same electrical charge for different current densities and the electrical charge at the transition points decreases with increasing pH.

Cupric ion concentration has little or no effect on the anodic dissolution of chalcopyrite. Ferrous ion over 5 g dm^{-3} produces a plateau value at 0.7 V vs. SHE, due to the preferred oxidation reaction of ferrous ion at the chalcopyrite surface; study is being carried out to obtain more comprehensive data to validate this conclusion. The temperature has no effect on the shape of the galvanostatic curves in the transient time-dependent region.

Galvanostatic measurements and empirical equations alone are not sufficient to study film formation [55]. To minimise this problem, additional studies are in progress in order to identify the steady state time-independent region of chalcopyrite in sulphuric acid solutions, investigate the reaction mechanism involved in the anodic dissolution of chalcopyrite, and further analyse the behaviour of chalcopyrite in the presence of cupric and ferrous ions and at high temperature.

It should be emphasised that although the dissolution of $CuFeS_2$ in sulphuric acid has been investigated for many years, there are still many unanswered questions regarding the conditions under which the passivating layers are formed on the chalcopyrite surface [56, 57]. Therefore, our aim is precisely to provide a more adequate description of this mineral passivation in acidic media.

References

1. Moskalyk RR, Alfantazi AM (2003) Miner Eng 16:893
2. Winkel L, Wochele J, Ludwig C, Alxneit I, Sturzenegger M (2008) Miner Eng 21:731
3. Baláž P (2000) Extractive metallurgy of activated minerals. Elsevier, Amsterdam
4. Burkin AR (2001) Chemical hydrometallurgy: theory and principles. Imperial College Press, London
5. Davenport WGL, King M, Schlessinger M, Biswas AK (2002) Extractive metallurgy of copper, 4th edn. Pergamon Press, London
6. Habashi F (1978) Chalcopyrite, its chemistry and metallurgy. McGraw-Hill, London
7. Sequeira CAC, Santos DMF, Chen Y, Anastassakis G (2008) Hydrometallurgy 92:135
8. Linge HG (1976) Hydrometallurgy 2:51
9. Antonijević MM, Bogdanović GD (2002) 34th IOC on Mining and Metallurgy, Bor Lake, Yugoslavia. Technical Faculty Bor, p 373
10. Hiroyoshi N, Miki H, Hirajima T, Tsunekawa M (2000) Hydrometallurgy 57:31
11. Hiroyoshi N, Arai M, Miki H, Tsunekawa M, Hirajima T (2002) Hydrometallurgy 63:257
12. Klauber C, Parker A, Bronswijk W, Watling H (2001) Int J Miner Process 62:65
13. Lu ZY, Jeffrey MI, Lawson F (2000) Hydrometallurgy 56:145
14. Lu ZY, Jeffrey MI, Lawson F (2000) Hydrometallurgy 56:189
15. Yu PH, Hansen CK, Wadsworth ME (1973) International symposium on hydrometallurgy, Chicago, Illinois, February 25–March 1. AIME, New York, p 375
16. Dixon DG (1995) Hydrometallurgy 39:337
17. Biegler T, Swift DA (1979) J Appl Electrochem 9:545
18. Gomez C, Figueroa M, Muñoz J, Blasquez ML, Ballester A (1996) Hydrometallurgy 43:331
19. Warren GW, Wadsworth ME, El-Raghy SH (1982) Metall Trans B 13:571
20. Elsherief AE (2002) Miner Eng 15:215
21. Prasad S, Pandey BD (1998) Miner Eng 11:763
22. Reddy RG (2003) Metall Mater Trans B 34:137
23. Choi IH, Yu PY (1999) Phys Status Solidi B 211:143
24. Crundwell FK (1988) Hydrometallurgy 21:155
25. De Alvarez CV, Cohen ML, Ley L, Kowalczyk SP, McFeely FR, Shirley DA, Grant RW (1974) Phys Rev B 10:596
26. Kumar V, Sastry BSR (2005) J Phys Chem Solids 66:99
27. Shuey RT (1975) Semiconducting ore minerals. Elsevier, New York
28. Cabri LJ (1973) Econ Geol 68:443
29. Dutrizac JE (1978) Metall Trans B 9:431
30. Dutrizac JE (1981) Metall Trans B 12:371
31. Dutrizac JE (1989) Can Metall Q 28:337
32. Dutrizac JE, MacDonald RJC (1973) Can Metall Q 12:409
33. Arce EM, González I (2002) Int J Miner Process 67:17
34. Pikna LA, Lux LA, Grygar TB (2006) Chem Pap 60:293
35. Lazaro I, Nicol MJ (2006) J Appl Electrochem 36:425
36. Tshilombo AF, Petersen J, Dixon DG (2002) Miner Eng 15:809
37. Petersen J, Dixon DG (2006) Hydrometallurgy 83:40
38. O'Connor DJ, Sexton BA, Smart RSC (eds) (1992) Surface analysis methods in materials science. Springer-Verlag, Berlin
39. Dixon DG, Mayne DD, Baxter KG (2008) Can Metall Q 47:327
40. Hauffe K (1965) Oxidation of metals. Plenum Press, New York
41. Young L (1961) Anodic oxide films. Academic Press, London
42. Holliday RI, Richmond WR (1990) J Electroanal Chem 288:83
43. Lu YP, Jiang XH, Feng QM, Ou LM, Zhang GF (2007) Chin J Nonfer Met 17:465
44. Mikhlin YL, Tomashevich YV, Asanov IP, Okotrub AV, Varnek VA, Vyalikh DV (2004) Appl Surf Sci 225:395
45. Cabrera N, Mott NF (1948-1949) Rep Prog Phys 12:163
46. Jelski DA, Nánai L, Vajtai R, Hevesi I, George TF (1993) Mater Sci Eng A 173:193
47. Ocal C, Ferrer S, Garcia N (1985) Surf Sci 163:335
48. Roy SK, Sircar SC (1981) J Electrochem Soc India 30:179
49. Ghez R (1973) J Chem Phys 58:1838
50. Sato N, Cohen M (1964) J Electrochem Soc 111:512
51. Maier J (2004) Physical chemistry of ionic materials, ions and electrons in solids. Wiley, Chichester, England
52. Sequeira CAC (1991) EMC'91: Non-ferrous metallurgy-present and future, Brussels, Belgium, September 15–20. Elsevier Applied Science, London
53. Sequeira CAC, Marquis FDS (1996) Environ Res Forum 1–2:395
54. Chao CY, Lin LF, MacDonald DD (1981) J Electrochem Soc 128:1187
55. Evans UR (1968) The corrosion and oxidation of metals, section 20–21. Arnold, London
56. Petersen J, Dixon DG (2002) Miner Eng 15:777
57. Viramontes-Gamboa G, Rivera-Vasquez BF, Dixon DG (2007) J Electrochem Soc 154:C299